Onset of buoyancy convection in a horizontal layer of a supercritical fluid heated from below

2004 J. Phys. A: Math. Gen. 37 7955

(http://iopscience.iop.org/0305-4470/37/32/009)

INSTITUTE OF PHYSICS PUBLISHING JOURNAL OF PHYSICS A: MATHEMATICAL AND GENERAL

J. Phys. A: Math. Gen. **37** (2004) 7955–7969 PII: S0305-4470(04)69569-2

Onset of buoyancy convection in a horizontal layer of a supercritical fluid heated from below

Toru Maekawa[1], **Koji Ishii**[1], **Yoshinori Shiroishi**[1] **and Hisao Azuma**[2]

[1] Bio-Nano Electronics Research Centre, Toyo University, 2100, Kujirai, Kawagoe, Saitama 350-8585, Japan
[2] Graduate School of Engineering, Osaka Prefecture University, 1-1, Gakuen-cho, Sakai, Osaka 599-8531, Japan

E-mail: trmkw@eng.toyo.ac.jp and toru.maekawa@physics.org

Received 30 September 2003, in final form 26 May 2004
Published 28 July 2004
Online at stacks.iop.org/JPhysA/37/7955
doi:10.1088/0305-4470/37/32/009

Abstract

We study the onset of buoyancy convection induced in a horizontal layer of a supercritical fluid heated from below. The physical situation, which we investigate, is as follows: the initial fluid temperature is set above the critical temperature. The following two cases are investigated: (a) the bottom surface temperature is raised at time zero and (b) a constant heat flux is given from the bottom surface at time zero. In both cases, the top surface temperature is kept at the initial fluid temperature. First, we analyse the temperature propagations on short time scales. We then investigate the onset conditions of buoyancy convection by linear stability analysis, by which the critical Rayleigh number and the critical wave number are obtained. We finally analyse the delay in the onset of buoyancy convection and the wave number of the convection induced in the supercritical fluid system. We find that power laws apply to the delay and the wave number with respect to the deviation of the initial fluid temperature from the critical temperature. The powers are, in fact, expressed by the critical exponents of some physical properties. This result suggests that the critical exponents can be estimated by measuring the onset times and wave numbers of convection experimentally.

PACS numbers: 44.25.+f, 47.20.−k, 83.60.Wc, 47.54.+r

1. Introduction

As a fluid system approaches the critical point, physical properties such as the specific heat and the isothermal compressibility diverge [1]. Because of the high specific heat, the thermal

diffusivity is very low, which suggests that thermal energy cannot be transferred quickly by thermal diffusion in critical fluids. It had been supposed that the temperature propagation speed is very low in critical fluids under microgravity conditions due to the reduction of both heat conduction and buoyancy convection. Unusual phenomena induced in critical fluids have been observed under both terrestrial and microgravity conditions. Nitsche and Straub [2] measured the specific heat at constant volume of SF_6 near the critical point under microgravity conditions. They observed fast temperature propagations even in microgravity. The propagation speed of temperature was much higher than that of thermal diffusion. Straub *et al* [3] carried out a spacelab experiment focusing on temperature propagations in critical SF_6, which was confined in a spherical container. After the temperature of the container wall was raised by approximately 15 mK, the temperature of the fluid rose very quickly. The temperature of the bulk fluid was almost constant and a very thin thermal boundary layer was established near the wall. Onuki *et al* [4] and Boukari *et al* [5] analysed this fast temperature propagation mechanism from a thermodynamical point of view. The temperature propagation mode was also investigated from a thermofluid dynamical point of view [6–10]. Now it is known that temperature propagates as acoustic waves in critical fluids, and this is called the *piston effect*. The propagation speed is $v_{\mathrm{wave}} = \sqrt{\gamma/(\rho\kappa_T)}$, where γ, ρ and κ_T are the ratio of specific heats, the density of a critical fluid and the isothermal compressibility, respectively. The dispersion relation between the frequency and the wave number of temperature waves under both terrestrial and zero-gravity conditions was also clarified [11].

Convection induced in critical fluids under terrestrial gravity conditions has also been investigated both numerically and experimentally [12–33]. Since the temperature coefficient of volume expansion increases and the thermal diffusivity decreases as fluids approach their critical points, strong buoyancy convection may be induced due to the very high Rayleigh number. The Prandtl number is also very large due to the very low thermal diffusivity, which may cause completely different convective instabilities. Giterman and Shteinberg [12, 13] studied convective instabilities in critical fluids and clarified the effect of Rayleigh–Bénard and Schwarzschild instabilities on the onset of convection, based on which Amiroudine *et al* [29] carried out numerical simulations of convection induced in a critical fluid confined in a square cavity. Carlès [27] derived the dispersion relation between the growth rates and wave numbers of perturbations as a function of time. The convective characteristics in critical fluids, however, have not yet been well understood.

In this paper, we focus on the onset of buoyancy convection induced in a supercritical fluid. The physical situation, which we investigate in this study, is illustrated in figure 1. A horizontal layer of a critical fluid is sandwiched between two parallel plates. Gravity acts downwards. The initial fluid temperature, T_i, is set above the critical temperature, T_c (figure 1(*a*)). We analyse the following two cases: (a) the bottom surface temperature is raised to T_b at t (time) $= 0$ (figure 1(*b*)); and (b) a constant heat flux, q, is given from the bottom surface at $t = 0$ (figure 1(*c*)). In both cases, the top surface temperature is kept at the initial fluid temperature, T_i. As we mentioned, the bulk temperature is raised quickly due to the temperature wave propagations. Since the thermal diffusivity is very low, which is caused by the large specific heat, the thermal boundary layers established at the top and bottom surfaces do not grow fast. As a result, a temperature distribution as shown in figure 1(*d*) is established in the early stages. In the following sections, we analyse the onset conditions and flow features of buoyancy convection induced in the system explained above. In section 2, we investigate the temperature propagations on short time scales. In section 3, we analyse the onset of buoyancy convection by linear stability analysis. We obtain the critical Rayleigh number and the critical wave number. In section 4, we investigate the dependence of the delay in the onset of convection after the heat input and the wave number of convection on the initial

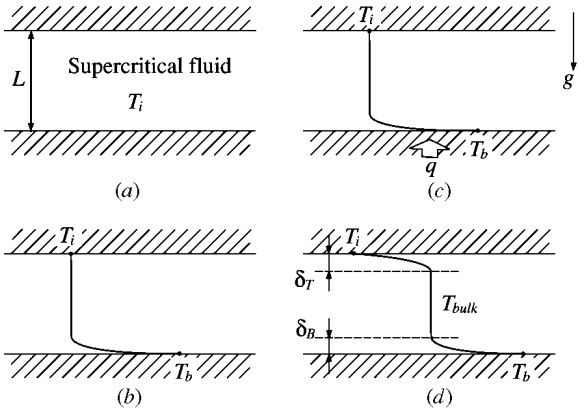

Figure 1. Physical situations. (*a*) A supercritical fluid is sandwiched between two horizontal plates. The initial fluid temperature, T_i, is set above the critical temperature, T_c. Gravitational acceleration acts downwards. We investigate the following two cases: (*b*) the temperature of the bottom surface is raised to T_b at t (time) $= 0$ and the top surface temperature is kept at T_i; and (*c*) a uniform heat flux, q, is given from the bottom surface at $t = 0$ and the top surface temperature is kept at T_i. In both cases, the bulk temperature, $T_{\rm bulk}$, is raised by the piston effect and thermal diffusion layers are established at the bottom and top surfaces. (*d*) A snapshot of a typical temperature distribution established in a supercritical fluid. The thicknesses of the thermal boundary layers, δ_B and δ_T, do not grow fast because of the low thermal diffusivity.

system temperature. In the final section, we summarize the result, which we obtained in this study.

2. Temperature propagations on short time scales

In this section, we analyse the temperature propagations on short time scales in the supercritical fluid system shown in figure 1 for the following two cases: (a) the bottom surface temperature is raised to T_b at $t = 0$ and (b) a constant heat flux, q, is given from the bottom surface at $t = 0$. In both cases, the top surface temperature is fixed at the initial fluid temperature, T_i. The bulk fluid temperature, $T_{\rm bulk}$, is supposed to rise by the piston effect in the following ways.

(a) *The bottom surface temperature is raised to T_b*:

$$T_{\rm bulk} = \tfrac{1}{2}\left\{(T_b + T_i) - (T_b - T_i)\,{\rm e}^{-\frac{t}{\tau_b}}\right\}. \tag{1}$$

(b) *A constant heat flux, q, is given from the bottom surface:*

$$T_{\rm bulk} = T_i + \frac{qL}{2\lambda}\left(1 - {\rm e}^{-\frac{t}{\tau_b}}\right), \tag{2}$$

where τ_b, L and λ are, respectively, the time constant for the bulk temperature to reach $(T_b + T_i)/2$ (see equation (1)) or $T_i + qL/2\lambda$ (see equation (2)), the depth of the fluid layer and the thermal conductivity of the fluid. The purpose of the analysis in this section is to estimate the time constant, τ_b, in terms of the initial system temperature, $\varepsilon \equiv T_i - T_c$, for the analysis of convective instabilities induced in the critical fluid system, which will be carried out in section 4. First of all, let us summarize the thermofluiddynamics equations [6, 11]:

- *Continuity equation:*

$$\frac{\partial \rho}{\partial t} + \frac{\partial}{\partial x_j}(\rho v_j) = 0, \tag{3}$$

where ρ and v_j are, respectively, the density and the velocity.

- *Momentum equation:*

$$\rho\left(\frac{\partial v_i}{\partial t}+v_j\frac{\partial v_i}{\partial x_j}\right)=-\frac{\partial p}{\partial x_i}+\frac{\partial \sigma_{ij}}{\partial x_j}+\rho g_i, \tag{4}$$

where p, g_i and σ_{ij} are, respectively, the pressure, the gravity vector and the viscous stress tensor defined as follows:

$$\sigma_{ij}\equiv\eta\left(\frac{\partial v_i}{\partial x_j}+\frac{\partial v_j}{\partial x_i}-\frac{2}{3}\delta_{ij}\frac{\partial v_k}{\partial x_k}\right). \tag{5}$$

Here, η is the dynamic viscosity, and the volume viscosity is not taken into account.

- *Transport equation of temperature:*

$$\frac{\partial T}{\partial t}+v_j\frac{\partial T}{\partial x_j}+\frac{\gamma-1}{\alpha_P}\frac{\partial v_j}{\partial x_j}=\frac{1}{\rho c_V}\left\{\frac{\partial}{\partial x_j}\left(\lambda\frac{\partial T}{\partial x_j}\right)+\sigma_{ij}\frac{\partial v_i}{\partial x_j}\right\}, \tag{6}$$

where T, γ, α_P and c_V are, respectively, the temperature, the ratio of specific heats, the temperature coefficient of volume expansion and the specific heat at constant volume.

- *Equation of state:*

$$\mathrm{d}p=\frac{1}{\rho\kappa_T}\mathrm{d}\rho+\frac{\alpha_P}{\kappa_T}\,\mathrm{d}T, \tag{7}$$

where κ_T is the isothermal compressibility.

We express the physical properties in terms of ε as follows:

$$c_P\sim\varepsilon^{-\alpha},\quad c_V\sim\varepsilon^{-\beta},\quad \kappa_T\sim\varepsilon^{-\gamma},\quad \alpha_P\sim\varepsilon^{-\Delta},\quad \lambda\sim\varepsilon^{-\Gamma},\quad \eta\sim\varepsilon^{-\chi}. \tag{8}$$

The actual values of c_P, c_V, κ_T, λ and η for the following numerical simulations are estimated based on those of CO_2 [34–37]. α_P is calculated from the van der Waals equation. In this case, $\alpha=1.2$ [34], $\beta=0.11$ [35], $\gamma=1.2$ [34], $\Delta=1.0$ (van der Waals), $\Gamma=0.6$ [36] and $\chi=0.04$ [37].

We solved numerically the above thermofluiddynamics equations by the control volume method [38], in which a staggered mesh system was employed and nonuniform mesh intervals were used so that the velocity, density, pressure and temperature fields near the boundaries could be calculated. The temperature propagations on very short time scales ($\sim\mu$s) are shown in figure 2, where $x=0$ and L (= 10 mm) correspond to the bottom and top surfaces, respectively. Figure 2(*a*) shows snapshots of the temperature propagations when the bottom surface temperature is raised by 10 mK at $t=0$, while figure 2(*b*) shows those when a constant heat flux of 100 W m^{-2} is given at $t=0$. As is clearly seen, temperature waves are created and travel between the two surfaces. Note that thermal diffusion layers at both surfaces are very thin on such short time scales because of the high specific heat. The temperature is raised each time the waves are reflected at the boundaries. The bulk temperature is raised, thanks to this fast temperature wave propagation and finally reaches $(T_b+T_i)/2$ in the case of the constant surface temperature conditions (see equation (1)) or $T_i+qL/2\lambda$ in the case of the constant heat flux conditions (see equation (2)). The time variations of the bulk temperature on millisecond scales and the dependence of the time constant for the bulk temperature to reach $(T_b+T_i)/2$ or $T_i+qL/2\lambda$ on the initial system temperature are shown in figure 3. The rising speed of the bulk temperature increases and therefore the time constant decreases as the system approaches the critical point when the bottom surface temperature is raised at time zero (figure 3(*a*)). On the other hand, when a constant heat flux is given from the bottom surface at time zero, the rising speed of the bulk temperature decreases as the initial system temperature approaches the critical temperature (figure 3(*b*)). However, since the bulk temperature rise at the steady state is lower due to the increase in the thermal conductivity (see equation (2)), the time constant in

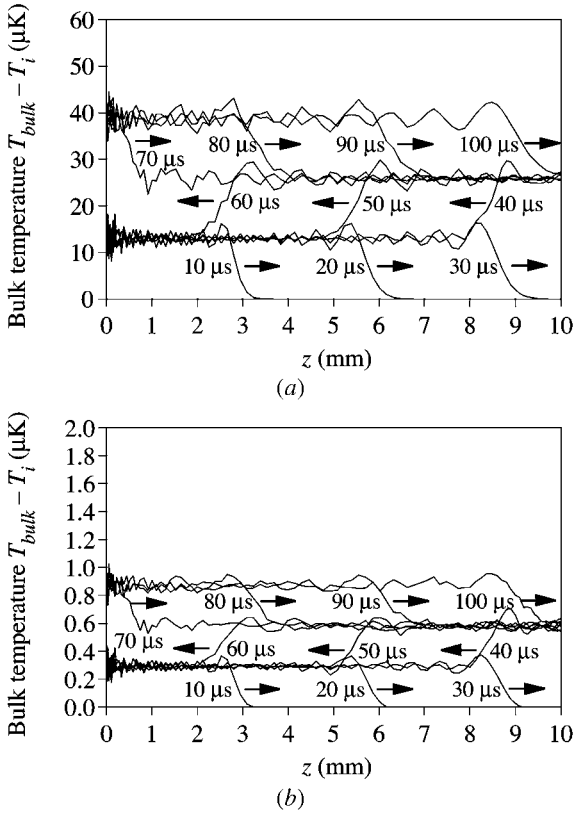

Figure 2. Temperature propagations on short time scales ($\sim\mu$s). The initial system temperature is 100 mK above the critical temperature. The system depth is 10 mm. The top surface temperature is kept at the initial system temperature. (*a*) The temperature of the bottom surface is raised by 10 mK; (*b*) a uniform heat flux of 100 W m^{-2} is given from the bottom surface.

the constant heat flux case also decreases as the system approaches the critical point. Power laws apply to the time constant with respect to ε in both cases. The values of the powers are the same irrespective of the differences in the boundary conditions.

Let us estimate the time constant theoretically. The third term on the left-hand side of equation (6) accounts for temperature wave propagations, and thermal energy is injected by diffusion via the first term on the right-hand side of equation (6). When the bottom surface temperature is raised by $T_b - T_i$, the following thermal energy balance applies on very short time scales, in which case the diffusion, dissipation, gravity and nonlinear convection terms are not predominant:

$$-\left.\frac{\partial T}{\partial z}\right|_{z=0} \approx \frac{\rho c_V}{\lambda}\frac{\gamma-1}{\alpha_P}|\Delta v|, \tag{9}$$

where $|\Delta v|$ is the amplitude of the velocity perturbation. Focusing on the wave propagations on short time scales, in which case the diffusion, dissipation, gravity and nonlinear terms do not have any significant effect, the relation between the amplitude of the velocity wave, $|\Delta v|$, and that of the temperature wave, $|\Delta T|$, is obtained as follows from equations (3)–(7):

$$|\Delta v| = \frac{\alpha_P}{\gamma-1}\sqrt{\frac{\gamma}{\rho\kappa_T}}|\Delta T|. \tag{10}$$

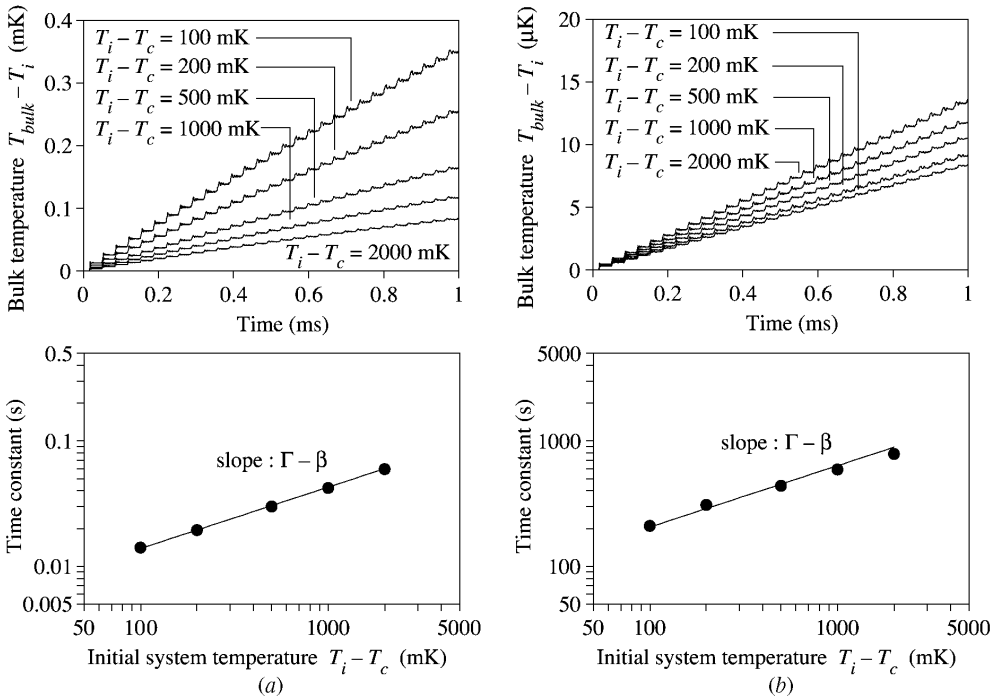

Figure 3. Time variations of the bulk temperature rise on millisecond scales and the dependence of the time constant of the bulk temperature rises on the initial system temperature. The system depth is 10 mm. (*a*) The temperature of the bottom surface is raised by 10 mK; (b) a uniform heat flux of 100 W m^{-2} is given from the bottom surface.

From equations (9) and (10), the amplitude of the temperature wave on short time scales is expressed as follows, assuming that the term $-(\partial T/\partial z)_{z=0}$ in equation (9) is almost constant on such short time scales so that the growth rate of the thermal diffusion layer, δ, is very low and the amount of the temperature rise is very small:

$$|\Delta T| = \frac{\lambda}{c_V}\sqrt{\frac{\kappa_T}{\rho\gamma}} \sim \varepsilon^{\frac{1}{2}\alpha+\frac{1}{2}\beta-\frac{1}{2}\gamma-\Gamma}. \tag{11}$$

This shows that the amplitude increases as the system approaches the critical point. Since the frequency of temperature wave reflections between the two boundaries, f, is $f = v_{\mathrm{wave}}/L$, where $v_{\mathrm{wave}} = \sqrt{\gamma/(\rho\kappa_T)}$ is the temperature wave speed, the rate of the bulk temperature rise, v_T, and the time constant, τ_b, are obtained as follows:

$$v_T = f \times |\Delta T| \sim \frac{\lambda}{c_V} \sim \varepsilon^{\beta-\Gamma}, \qquad \tau_b = \frac{T_b - T_i}{2v_T} \sim \varepsilon^{\Gamma-\beta}. \tag{12}$$

The time constant for the bulk temperature rise decreases as the system approaches the critical point. The power, $\Gamma - \beta$, coincides with that obtained by the numerical simulation (see figure 3(*a*)).

When a constant heat flux, q, is given at the bottom surface, the following relations are derived in the same manner:

$$q = -\lambda \left.\frac{\partial T}{\partial z}\right|_{z=0} \approx \rho c_V \frac{\gamma - 1}{\alpha_P}|\Delta v|. \tag{13}$$

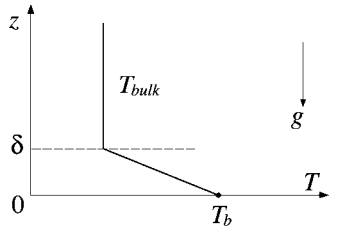

Figure 4. Initial conditions. The fluid is at rest initially. The bulk temperature, $T_{\rm bulk}$, is constant and a linear temperature distribution is established in the thermal diffusion layer, the thickness of which is δ. Gravity acts downwards.

From equations (10) and (13), the amplitude of the temperature wave is obtained as follows:

$$|\Delta T| = \frac{1}{c_V}\sqrt{\frac{\kappa_T}{\rho\gamma}} \sim \varepsilon^{\frac{1}{2}\alpha+\frac{1}{2}\beta-\frac{1}{2}\gamma}. \tag{14}$$

The amplitude of the temperature wave decreases as the system approaches the critical point as shown in figure 3(*b*). The rate of the bulk temperature rise, v_T, and the time constant, τ_b, are obtained as follows:

$$v_T = f \times |\Delta T| \sim \frac{1}{c_V} \sim \varepsilon^{\beta}, \qquad \tau_b = \frac{qL}{2\lambda v_T} \sim \varepsilon^{\Gamma-\beta}. \tag{15}$$

The time constant for the bulk temperature rise also decreases as the system approaches the critical point and coincides with that obtained by the numerical simulation (see figure 3(*b*)). In other words, the assumptions made in the above theoretical analysis on such short time scales are correct. The values of the powers are the same irrespective of the differences in the boundary conditions (see equations (12) and (15)).

3. Onset conditions of buoyancy convection

In this section, we carry out a linear stability analysis of buoyancy convection of the system described in section 1 (see figure 1). Here, we focus on the case when thermal convection is induced by Rayleigh–Bénard instability in the thermal boundary layer. Whereas a linear temperature distribution is established throughout the horizontal fluid layer by heat conduction and convection occurs if the Rayleigh number exceeds the critical value in the case of normal fluids [39], the temperature distribution as shown in figure 1(*d*) is established due to the piston effect and the slow development of thermal diffusion layers in the case of supercritical fluids. Because of the temperature distribution shown in figure 1(*d*), buoyancy convection may be driven upwards from the bottom thermal boundary layer and downwards from the top thermal boundary layer although the top surface is not externally cooled. The physical situations analysed here are basically the same as those analysed by Carlès [27] and Khouri and Carlès [33]. As we mentioned, Carlès [27] derived the dispersion relation between the growth rates and the wave numbers of perturbations as a function of time. Amiroudine *et al* [29] carried out numerical simulations of convection induced in a critical fluid in a square cavity heated from below, but the flow patterns were definitely affected by the vertical walls because of the small aspect ratio (horizontal width/vertical depth). In this section, on the other hand, we obtain the marginal conditions of the onset of buoyancy convection from the bottom thermal boundary layer of an infinite horizontal layer, that is, the critical Rayleigh number and the critical wave number. The initial conditions are modelled as follows (see also figure 4): the initial velocity

in the fluid is zero and the following initial temperature distribution, T_0, is established:

$$T_0 = \begin{cases} -\frac{T_b - T_{\text{bulk}}}{\delta} z + T_b & (0 \leqslant z \leqslant \delta) \\ T_{\text{bulk}} (\delta < z), \end{cases} \tag{16}$$

where T_b, T_{bulk} and δ are, respectively, the bottom surface temperature, the bulk fluid temperature and the thickness of the thermal diffusion layer (see figure 4). Since we focus on the onset of convection, in which case the time scales are much longer than those of the temperature wave propagations, we omit the velocity divergence terms in equations (5) and (6). Instead, we employ the Boussinesq approximation to take into account the buoyancy effect. It was, in fact, proved theoretically that the piston effect does not have any influence on the onset of buoyancy convection [25, 27]. We superimpose perturbations on the initial velocity and temperature as follows:

$$v_i = 0 + \tilde{v}_i, \qquad T = T_0 + \tilde{T} \tag{17}$$

where $\sim$ represents the perturbation. Substituting the velocity and temperature values (equation (17)) in the thermofluiddynamics equations, employing the Boussinesq approximation and omitting the velocity divergence terms and the second-order perturbation terms, the following nondimensional linear equations are derived [39]:

$$\frac{\partial}{\partial \tau}(\nabla^2 V_Z) = \nabla^4 V_Z + \frac{Ra}{Pr} \nabla_{\text{II}}^2 \theta, \tag{18}$$

where ∇_{II}^2 is the two-dimensional Laplacian on the horizontal plane.

$$\frac{\partial \theta}{\partial \tau} = \begin{cases} V_Z + \frac{1}{Pr} \nabla^2 \theta & (0 \leqslant Z \leqslant 1) \\ \frac{1}{Pr} \nabla^2 \theta & (1 < Z). \end{cases} \tag{19}$$

In equations (18) and (19), the coordinate x_i, the time t, the z-component of the velocity, $\tilde{v}_z$, and the temperature$\tilde{T}$ are nondimensionalized as follows:

$$X_i \equiv \frac{x_i}{\delta}, \qquad \tau \equiv \frac{t}{\delta^2/\nu}, \qquad V_Z \equiv \frac{\tilde{v}_z}{\nu/\delta}, \qquad \theta \equiv \frac{\tilde{T}}{T_b - T_{\text{bulk}}}, \tag{20}$$

where $\nu \equiv \eta/\rho$ is the kinematic viscosity. Note that the thickness of the thermal diffusion layer, δ, is used as the characteristic length for the nondimensionalization. Pr and Ra in equations (18) and (19) are, respectively, the Prandtl number and the Rayleigh number:

$$Pr \equiv \frac{\nu}{a}, \qquad Ra \equiv \frac{\alpha_P g \Delta T \delta^3}{a \nu}, \tag{21}$$

where a and g are the thermal diffusivity and the gravitational acceleration, respectively, and $\Delta T \equiv T_b - T_{\text{bulk}}$. Note that, as we explained, the Rayleigh number is defined using δ.

We carry out harmonic analysis based on the following solutions for the velocity and temperature perturbations:

$$\begin{pmatrix} V_Z \\ \theta \end{pmatrix} = \begin{pmatrix} V(Z) \\ \Theta(Z) \end{pmatrix} \exp(\sigma \tau - \mathrm{i} K_X X - \mathrm{i} K_Y Y), \tag{22}$$

where K_X and K_Y are, respectively, the X- and Y-components of the nondimensional wave numbers ($K_X \equiv k_x \delta$, $K_Y \equiv k_y \delta$, where k_x and k_y are the wave numbers) and $\sigma = \sigma_R + \mathrm{i}\sigma_{\text{I}}$. Substituting equation (22) in the governing equations (18) and (19), the following equations are obtained:

$$\{\sigma (D^2 - K^2) - (D^2 - K^2)^2\} V + \frac{Ra}{Pr} K^2 \Theta = 0, \tag{23}$$

$$\begin{aligned} V - \left\{\sigma - \frac{1}{Pr}(D^2 - K^2)\right\}\Theta = 0 \qquad & (0 \leqslant Z \leqslant 1) \\ \left\{\sigma - \frac{1}{Pr}(D^2 - K^2)\right\}\Theta = 0 \qquad & (1 < Z), \end{aligned} \tag{24}$$

where $D \equiv \mathrm{d}/\mathrm{d}Z$ and $K^2 \equiv K_X^2 + K_Y^2$. The boundary conditions are

$$V = DV = 0, \qquad \theta = 0 \qquad \text{at} \quad Z = 0, \infty. \tag{25}$$

We expand V and Θ by the trial functions $f_i(Z)$ and $g_i(Z)$:

$$V(Z) = \sum_i \alpha_i f_i(Z), \qquad \Theta(Z) = \sum_i \beta_i g_i(Z), \tag{26}$$

where α_i and β_i are the coefficients. We use the following functions for $f_i(Z)$ and $g_i(Z)$ to satisfy the boundary conditions:

$$f_i(Z) = Z^{i+1}\,\mathrm{e}^{-Z}, \qquad g_i(Z) = Z^i\,\mathrm{e}^{-Z}. \tag{27}$$

Substituting equation (26) in equations (23) and (24) and employing the Galerkin method, the following eigenvalue matrix equation is obtained:

$$A_3^{-1}(\sigma A_1 + A_2)B_1^{-1}(Pr\sigma B_2 + B_3)\beta = Ra\beta, \tag{28}$$

where Ra is the eigenvalue and $\beta \equiv (\beta_1, \beta_2, \beta_3, \ldots)^T$ is the eigenvector. Matrices A_1, A_2, A_3, B_1, B_2 and B_3 are defined as follows:

$$A_1 \equiv \int_0^\infty (D\delta f_m)(Df_i)\,\mathrm{d}Z + K^2 \int_0^\infty \delta f_m f_i\,\mathrm{d}Z,$$

$$A_2 \equiv \int_0^\infty (D^2\delta f_m)(D^2 f_i)\,\mathrm{d}Z + 2K^2 \int_0^\infty (D\delta f_m)(Df_i)\,\mathrm{d}Z + K^4 \int_0^\infty \delta f_m f_i\,\mathrm{d}Z,$$

$$A_3 \equiv K^2 \int_0^\infty \delta f_m g_i\,\mathrm{d}Z, \qquad B_1 \equiv \int_0^1 \delta g_m f_i\,\mathrm{d}Z, \qquad B_2 \equiv \int_0^\infty \delta g_m g_i\,\mathrm{d}Z,$$

$$B_3 \equiv \int_0^\infty (D\delta g_m)(Dg_i)\,\mathrm{d}Z + K^2 \int_0^\infty \delta g_m g_i\,\mathrm{d}Z.$$

At the neutral state, $\sigma_R = 0$. We calculated the critical Rayleigh number changing σ_I under different combinations of the Prandtl number, Pr, and wave number, K, and found that $\sigma_\mathrm{I} = 0$ always gives the minimum Rayleigh number. In other words, overstability does not occur at the marginal state. The neutral curve for $\sigma_\mathrm{I} = 0$ is shown in figure 5, where the minimum value gives the critical Rayleigh number, and the wave number corresponding to the critical Rayleigh number is the critical wave number. We expanded the solutions using up to 12 trial functions (see equations (26) and (27)) and confirmed that the significant figure of 3 was achieved in both the critical Rayleigh number and the critical wave numbers. The critical Rayleigh number, Ra_c, and the corresponding nondimensional critical wave number, K_c, are, respectively, 0.434 and 0.356. The isotherms obtained from the temperature eigenvectors are shown in figure 6. Very narrow thermal plumes are driven from the boundary layer once the Rayleigh number reaches the critical value. Note that in the case of an infinite horizontal layer of a normal fluid sandwiched between two rigid walls, the critical Rayleigh number and the critical wave number are approximately 1708 and 3.117, respectively, where the Rayleigh number and the wave number are nondimensionalized using the distance between the two plates [39]. Let us estimate the thickness of the boundary layer, δ, when thermal convection occurs in supercritical CO_2. When, for instance, $T_i - T_c = 1000$ mK and $T_b - T_\mathrm{bulk} = 10$ mK, $\delta \approx 0.62$ μm and therefore the wavelength between neighbouring plumes, $\lambda_\mathrm{plume} = 2\pi\delta/K_c$,

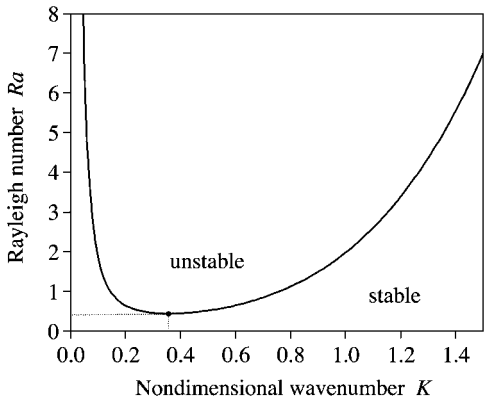

Figure 5. Neutral curve. The minimum value gives the critical Rayleigh number, Ra_c, and the corresponding wave number is the critical wave number, K_c; $Ra_c = 0.434$ and $K_c = 0.356$.

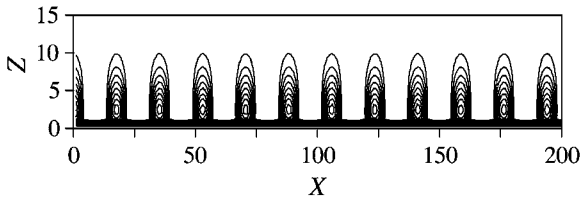

Figure 6. Isotherms of thermal plumes calculated from the temperature eigenvector. Plumes of a short wavelength are driven from the thermal boundary layer.

is approximately 11 μm. When $T_i - T_c = 100$ mK, and $T_b - T_{\text{bulk}} = 10$ mK, $\delta \approx 0.18$ μm and $\lambda_{\text{plume}} \approx 3.3$ μm. The above examples show that as long as the gap between the top and bottom surfaces is not of the order of micrometres, buoyancy convection occurs from the thermal boundary layers before a linear temperature distribution is established across the whole fluid layer [25, 27, 33].

4. Convective characteristics

In this section, we analyse the convective characteristics induced in supercritical fluids. As we explained, the physical situation is as follows (see figure 1). The initial fluid temperature is T_i, which is slightly higher than the critical temperature T_c. The bottom surface temperature is raised to T_b or a uniform heat flux, q, is given from the bottom surface at time zero, and in both cases the top surface temperature is kept at the initial fluid temperature. The bulk fluid temperature is raised by the piston effect (see section 2) and the thermal boundary layers at the top and bottom surfaces grow very slowly due to the low thermal diffusivity. Under the above circumstances, thermal convection is driven upwards from the bottom boundary layer and downwards from the top boundary layer once the onset conditions are satisfied. In general, thermal convection occurs when the corrected Rayleigh number, Ra^{Corr}, reaches the critical Rayleigh number, Ra_c, in critical fluids [25, 29, 30, 32]:

$$Ra^{\text{Corr}} \equiv Ra \times \left(1 - a_g \frac{\delta}{\Delta T}\right) = Ra_c, \tag{29}$$

where $a_g \equiv (\partial T/\partial p)_S \rho g = g\alpha_P T/c_P$ [40]. However, as we showed in section 3, the thickness of the thermal boundary layer, δ, is very short and, as a result, the correction term,

$a_g\delta/\Delta T$, becomes much smaller than 1 [29, 32]. Therefore, in this study, we assume that the correction term can be omitted as far as the onset of convection from thin boundary layers is concerned [25] and that buoyancy convection is induced when the Rayleigh number Ra reaches the critical Rayleigh number Ra_c.

The temperature difference between the bottom surface and the bulk fluid, $\Delta T_B \equiv T_b - T_{\text{bulk}}$, changes with time and the thickness of the bottom thermal boundary layer, δ_B, increases with an increase in time. Therefore, when the Rayleigh number reaches the critical value, Ra_c, buoyancy convection occurs upwards from the bottom boundary layer:

$$Ra_B \equiv \frac{\alpha_P g \Delta T_B \delta_B^3}{a\nu} = Ra_c, \tag{30}$$

where Ra_c is the critical Rayleigh number, which we obtained in section 3. The wave number of buoyancy convection from the bottom boundary layer is

$$k_{B,c} \equiv \frac{K_c}{\delta_B}, \tag{31}$$

where K_c is the nondimensional critical wave number, which we also obtained in section 3. Let us focus on thermal convection from the top surface. Both the temperature difference between the bulk fluid and the top surface, $\Delta T_T = T_{\text{bulk}} - T_i$, and the thickness of the top thermal boundary layer, δ_T, increase with time, and when the Rayleigh number reaches the critical value, buoyancy convection occurs downwards from the top boundary layer:

$$Ra_T \equiv \frac{\alpha_P g \Delta T_T \delta_T^3}{a\nu} = Ra_c. \tag{32}$$

The wave number of convection from the top boundary layer is

$$k_{T,c} \equiv \frac{K_c}{\delta_T}. \tag{33}$$

4.1. Buoyancy convection when the bottom surface temperature is raised

First, we analyse the convective characteristics when the bottom surface temperature is raised to T_b at time zero (see figure 1(*b*)). Since the temperature of the bulk fluid, T_{bulk}, is raised by the piston effect as shown in equation (1), the temperature difference between the bottom surface and the bulk fluid, $\Delta T_B = T_b - T_{\text{bulk}}$, and that between the bulk fluid and the top surface, $\Delta T_T = T_{\text{bulk}} - T_i$, change with time as follows:

$$\Delta T_B \equiv T_b - T_{\text{bulk}} = \tfrac{1}{2}(T_b - T_i)\left(1 + \mathrm{e}^{-\frac{t}{\tau_b}}\right), \tag{34}$$

$$\Delta T_T \equiv T_{\text{bulk}} - T_i = \tfrac{1}{2}(T_b - T_i)\left(1 - \mathrm{e}^{-\frac{t}{\tau_b}}\right), \tag{35}$$

where τ_b is the time constant (see equation (12)). We estimate the onset of buoyancy convection from the bottom and top boundary layers based on equations (30)–(33). The thermal diffusivity, a, and the thickness of a thermal boundary layer, δ, are expressed as follows:

$$a \equiv \frac{\lambda}{\rho c_V} \sim \varepsilon^{\beta-\Gamma}, \qquad \delta \sim \sqrt{at} \sim \varepsilon^{\frac{1}{2}(\beta-\Gamma)} t^{\frac{1}{2}}. \tag{36}$$

Substituting α_P (equation (8)), ΔT_B (equation (34)), ΔT_T (equation (35)), a (equation (36)) and δ (equation (36)) in equations (30) and (32), the time variations of the Rayleigh numbers are expressed as follows:

$$Ra_B \sim \alpha_P \Delta T_B \delta_B^3 a^{-1}\nu^{-1} \sim \alpha_P \delta_B^3 a^{-1}\nu^{-1} \sim \varepsilon^{\frac{1}{2}\beta - \frac{1}{2}\Gamma - \Delta + \chi} t^{\frac{3}{2}}, \tag{37}$$

$$Ra_T \sim \alpha_P \Delta T_T \delta_T^3 a^{-1} \nu^{-1} \sim \alpha_P \delta_T^3 a^{-1} \nu^{-1} \sim \varepsilon^{\frac{1}{2}\beta - \frac{1}{2}\Gamma - \Delta + \chi} t^{\frac{3}{2}}, \tag{38}$$

where $e^{-t/\tau_b} \approx 0$ is applied since τ_b is of the order of 0.01 s (see figure 3(a)) and the onset time of convection is of the order of several seconds [29, 31]. The Rayleigh numbers Ra_B and Ra_T increase with time and when the Rayleigh numbers reach the critical number Ra_c, which we obtained in section 2, buoyancy convection occurs. Therefore, the onset time of thermal convection from the bottom boundary layer, t_B, and that from the top boundary layer, t_T, are expressed as follows:

$$t_B \sim \varepsilon^{-\frac{1}{3}\beta + \frac{1}{3}\Gamma + \frac{2}{3}\Delta - \frac{2}{3}\chi}, \tag{39}$$

$$t_T \sim \varepsilon^{-\frac{1}{3}\beta + \frac{1}{3}\Gamma + \frac{2}{3}\Delta - \frac{2}{3}\chi}. \tag{40}$$

Thus, we obtained power relations between the onset times of thermal convection from the bottom and top boundary layers, t_B and t_T, and the difference between the initial system temperature and the critical temperature, ε. The powers are the same for both t_B and t_T. Generally speaking, the onset time of buoyancy convection is delayed more and more as the system temperature deviates from the critical temperature. From equations (31) and (33), the wave numbers of buoyancy convection from the bottom and top boundary layers, $k_{B,c}$ and $k_{T,c}$, are obtained as follows:

$$k_{B,c} \sim \delta_B^{-1} \sim \varepsilon^{\frac{1}{2}(\Gamma - \beta)} t_B^{-\frac{1}{2}} \sim \varepsilon^{-\frac{1}{3}\beta + \frac{1}{3}\Gamma - \frac{1}{3}\Delta + \frac{1}{3}\chi}, \tag{41}$$

$$k_{T,c} \sim \delta_T^{-1} \sim \varepsilon^{\frac{1}{2}(\Gamma - \beta)} t_T^{-\frac{1}{2}} \sim \varepsilon^{-\frac{1}{3}\beta + \frac{1}{3}\Gamma - \frac{1}{3}\Delta + \frac{1}{3}\chi}. \tag{42}$$

Power laws also apply to the wave numbers with respect to ε. The wave number increases as the system approaches the critical point. In other words, the wavelength between plumes becomes shorter as the initial system temperature approaches the critical temperature.

4.2. Buoyancy convection when a constant heat flux is given from the bottom surface

Let us investigate the flow features when a uniform heat flux, q, is given from the bottom surface at time zero (see figure 1(c)). In this case, the difference between the bottom surface temperature, T_b, and bulk temperature, T_{bulk}, increases following Fourier's law as follows:

$$\Delta T_B \equiv T_b - T_{\mathrm{bulk}} = \frac{q}{\lambda} \delta_B. \tag{43}$$

Since the bulk temperature is supposed to change as shown in equation (2), the temperature difference between the bulk fluid and the top surface, $\Delta T_T = T_{\mathrm{bulk}} - T_i$, changes with time as follows:

$$\Delta T_T \equiv T_{\mathrm{bulk}} - T_i = \frac{qL}{2\lambda} \left(1 - e^{-\frac{t}{\tau_b}}\right). \tag{44}$$

We can again estimate the onset of thermal convection from the bottom and top boundary layers based on equations (30)–(33). The time variations of the Rayleigh numbers are expressed as follows:

$$Ra_B \sim \alpha_P \Delta T_B \delta_B^3 a^{-1} \nu^{-1} \sim \alpha_P q \lambda^{-1} \delta_B \delta_B^3 a^{-1} \nu^{-1} \sim \varepsilon^{\beta - \Delta + \chi} q t^2, \tag{45}$$

$$Ra_T \sim \alpha_P \Delta T_T \delta_T^3 a^{-1} \nu^{-1} \sim \alpha_P q \lambda^{-1} t \tau_b^{-1} \delta_T^3 a^{-1} \nu^{-1} \sim \varepsilon^{\frac{3}{2}\beta - \frac{1}{2}\Gamma - \Delta + \chi} q t^{\frac{5}{2}}, \tag{46}$$

where $e^{-t/\tau_b} \approx 1 - t/\tau_b$ is applied since τ_b is very large (see figure 3(b)) compared to the onset time of convection [29, 31]. Therefore, the onset time of buoyancy convection from the bottom boundary layer, t_B, and that from the top boundary layer, t_T, are obtained as follows:

$$t_B \sim q^{-\frac{1}{2}} \varepsilon^{-\frac{1}{2}\beta + \frac{1}{2}\Delta - \frac{1}{2}\chi}, \tag{47}$$

$$t_T \sim q^{-\frac{2}{5}} \varepsilon^{-\frac{3}{5}\beta + \frac{1}{5}\Gamma + \frac{2}{5}\Delta - \frac{2}{5}\chi}. \tag{48}$$

From equations (31) and (33), the wave numbers of buoyancy convection from the bottom and top boundary layers, $k_{B,c}$ and $k_{T,c}$, respectively, are obtained as follows:

$$k_{B,c} \sim \delta_B^{-1} \sim \varepsilon^{\frac{1}{2}(\Gamma-\beta)} t_B^{-\frac{1}{2}} \sim q^{\frac{1}{4}} \varepsilon^{-\frac{1}{4}\beta+\frac{1}{2}\Gamma-\frac{1}{4}\Delta+\frac{1}{4}\chi}, \tag{49}$$

$$k_{T,c} \sim \delta_T^{-1} \sim \varepsilon^{\frac{1}{2}(\Gamma-\beta)} t_T^{-\frac{1}{2}} \sim q^{\frac{1}{5}} \varepsilon^{-\frac{1}{5}\beta+\frac{2}{5}\Gamma-\frac{1}{5}\Delta+\frac{1}{5}\chi}. \tag{50}$$

Thus, we also derived power relations. The onset time of thermal plumes and the wave number decrease as the initial system temperature approaches the critical temperature.

In summary, power laws apply to the onset times of thermal convection from the bottom and top boundary layers and to the wave numbers of convection with respect to $\varepsilon \equiv T_i - T_c$ in both constant temperature and constant heat flux cases. The powers are expressed by the critical exponents of several physical properties. Thermal plumes of large wave numbers induced from the bottom surface have been observed by numerical simulations [22, 29–32] and those from the top surface have also been shown numerically [22, 29–31]. Convective instabilities are affected by side walls. The critical Rayleigh number is, in general, raised when the aspect ratio of the fluid layer (width/height) becomes low. But since the wavelength between the thermal plumes is very short in the case of critical fluids, the side wall or end effect may not be so serious as the ordinary Rayleigh–Bénard instability. As is well known, a direct measurement of physical properties of near-critical fluids under terrestrial gravitational conditions is very difficult due to the piston effect, gravity and thermal convection. However, the above power relations suggest that the critical exponents of some physical properties can be estimated by measuring the onset times and wave numbers of thermal plumes driven from the bottom and top thermal boundary layers. What is more, the present analysis can be easily extended to different heating conditions by changing the boundary conditions (see equations (1) and (2)), in which case the values of the powers may be changed. According to our recent preliminary experiment using supercritical CO_2, a power relation between the delay in the onset of buoyancy plumes and ε and another relation between the wave number and ε can be clearly observed, the result of which will be presented soon. We should mention that the power laws may not apply when the system temperature is very close to the critical temperature since the macroscopic thermodynamic treatment may not be valid any more. The power laws also disappear when the initial system temperature is set far from the critical temperature, in which case a linear temperature distribution is established across the fluid layer due to the fast thermal diffusion and therefore the present situation is changed to an ordinary Rayleigh–Bénard problem.

5. Conclusions

We theoretically studied convective instability induced in a horizontal layer of a critical fluid and obtained the following results. (a) We carried out linear stability analysis of the onset of thermal convection in a critical fluid system and obtained the critical Rayleigh number, Ra_c, and the critical nondimensional wave number, K_c; $Ra_c = 0.434$ and $K_c = 0.356$, where the Rayleigh number and the wave number are nondimensionalized by the thickness of the thermal boundary layer. (b) We investigated the delay in the onset of convection and the actual wave number of thermal convection induced in the fluid layer and found that the following power laws apply to the delay and the wave number depending on the initial thermal conditions: (1) the case when the bottom wall temperature is raised at time zero: $t_B \sim t_T \sim \varepsilon^{-\frac{1}{3}\beta+\frac{1}{3}\Gamma+\frac{2}{3}\Delta-\frac{2}{3}\chi}$, $k_{B,c} \sim k_{T,c} \sim \varepsilon^{-\frac{1}{3}\beta+\frac{1}{3}\Gamma-\frac{1}{3}\Delta+\frac{1}{3}\chi}$, where t_B is the delay in the onset of thermal convection from the bottom thermal boundary layer; t_T is the delay in the onset of thermal convection from the top boundary layer; $k_{B,c}$ is the wave number of thermal convection

from the bottom boundary layer; $k_{T,c}$ is the wave number of thermal convection from the top boundary layer; β, Γ, Δ and χ are the critical exponents of the specific heat at constant volume, the thermal conductivity, the temperature coefficient of volume expansion and the kinematic viscosity, respectively; and ε is the difference between the initial fluid temperature and the critical temperature; (2) the case when a constant heat flux is given from the bottom wall at time zero: $t_B \sim q^{-\frac{1}{2}}\,\varepsilon^{-\frac{1}{2}\beta+\frac{1}{2}\Delta-\frac{1}{2}\chi}$, $t_T \sim q^{-\frac{2}{5}}\,\varepsilon^{-\frac{3}{5}\beta+\frac{1}{5}\Gamma+\frac{2}{5}\Delta-\frac{2}{5}\chi}$, $k_{B,c} \sim q^{\frac{1}{4}}\,\varepsilon^{-\frac{1}{4}\beta+\frac{1}{2}\Gamma-\frac{1}{4}\Delta+\frac{1}{4}\chi}$, $k_{T,c} \sim q^{\frac{1}{5}}\,\varepsilon^{-\frac{1}{5}\beta+\frac{2}{5}\Gamma-\frac{1}{5}\Delta+\frac{1}{5}\chi}$, where q is the heat flux from the bottom surface. The power relations suggest that the critical exponents of some physical properties can be estimated by measuring the onset times and wave numbers of thermal plumes driven from the bottom and top thermal boundary layers. The present analysis can be easily extended to different heating conditions, depending on which different powers are obtained.

Acknowledgments

We have received the following research funds: (a) the Grant for 21st Century Centre of Excellence Programmes organized by the Ministry of Education, Culture, Sports, Science and Technology (MEXT), Japan, since 2003; (b) the Grant for High Tech Research Centres organized by MEXT since 1996; and (c) the Grant-in-Aid for Scientific Research organized by the Japanese Society for the Promotion of Science (JSPS), since 2002.

References

[1] Stanley H E 1971 *Introduction to Phase Transition and Critical Phenomena* (Oxford: Oxford University Press)
[2] Nitsche K and Straub J 1987 *Proceedings of 6th European Symposium on Material Sciences under Microgravity Conditions (Bordeaux, France, 1986)* (Paris: European Space Agency) p 109 SP-256
[3] Straub J, Eicher L and Haupt A 1995 *Phys. Rev.* E **51** 5556
[4] Onuki A, Hao H and Ferrell A 1990 *Phys. Rev.* A **41** 2256
[5] Boukari H, Shaumeyer J N, Briggs M E and Gammon R W 1990 *Phys. Rev.* A **41** 2260
[6] Zappoli Z, Bairy D, Garrabos Y, Le Neindre B, Guenoun P and Beysens D 1990 *Phys. Rev.* A **41** 2264
[7] Zappoli B 1992 *Phys. Fluids* A **4** 1040
[8] Zappoli B and Durand-Daubin A 1994 *Phys. Fluids* **6** 1929
[9] Zappoli B and Carlès P 1995 *Eur. J. Mech.* B **14** 41
[10] Zappoli B and Carlès P 1996 *Physica* D **89** 381
[11] Ishii K, Maekawa T, Azuma H, Yoshihara S and Onishi M 1998 *Appl. Phys. Lett.* **72** 16
[12] Giterman M Sh and Shteinberg V A 1970 *J. Appl. Math. Mech.* **34** 305
[13] Giterman M Sh and Shteinberg V A 1970 *High Temp.—High Pressures* **8** 754
[14] Klein H and Feuerbacher B 1987 *Phys. Lett.* A **123** 183
[15] Boukari H, Pego R L and Gammon R W 1995 *Phys. Rev.* E **52** 1614
[16] Straub J, Eicher L and Haupt A 1995 *Int. J. Thermophys.* **16** 1051
[17] Bonetti M, Perrot F, Beysens D and Garrabos Y 1995 *Int. J. Thermophys.* **16** 1059
[18] Zhong F and Meyer H 1995 *Phys. Rev.* E **51** 3223
[19] Zappoli B, Amiroudine S, Carlès P and Ouazzani J 1996 *J. Fluid Mech.* **316** 53
[20] Zhong F and Meyer H 1996 *Phys. Rev.* E **53** 5935
[21] Garrabos Y, Bonetti M, Beysens D, Perrot F, Föhlich T, Carlès P and Zappoli B 1998 *Phys. Rev.* E **57** 5665
[22] Raspo I, Gilly B, Amiroudine S, Bontoux P and Zappoli B 1999 *J. Chim. Phys.* **96** 1059
[23] Zappoli B, Jounet A, Amiroudine S and Mojtabi A 1999 *J. Fluid Mech.* **388** 389
[24] Azuma H, Yoshihara S, Onishi M, Ishii K, Masuda S and Maekawa T 1999 *Int. J. Heat Mass Transfer* **42** 771
[25] Carlès P and Ugurtas B 1999 *Physica* D **126** 69
[26] Bailly D and Zappoli B 2000 *Phys. Rev.* E **62** 2353
[27] Carlès P 2000 *Physica* D **147** 36
[28] Kogan A B and Meyer H 2001 *Phys. Rev.* E **63** 056310
[29] Amiroudine S, Bontoux P, Larroude P, Gilly B and Zappoli B 2001 *J. Fluid Mech.* **442** 119
[30] Chiwata Y and Onuki A 2001 *Phys. Rev. Lett.* **87** 144301
[31] Maekawa T, Ishii K, Ohnishi M and Yoshihara S 2002 *Adv. Space Res.* **29** 589

[32] Furukawa A and Onuki A 2002 *Phys. Rev.* E **66** 016302
[33] Khouri L E and Carlès P 2002 *Phys. Rev.* E **66** 066309
[34] Swinney H L and Henry D L 1973 *Phys. Rev.* A **8** 2586
[35] Haupt A and Straub J 1999 *Phys. Rev.* E **59** 1795
[36] Sengers J V and Keyes P H 1971 *Phys. Rev. Lett.* **26** 70
[37] Berg R F and Moldover M R 1990 *J. Chem. Phys.* **93** 1926
[38] Patanker S V and Spalding D B 1972 *Int. J. Heat Mass Transfer* **15** 1787
[39] Chandrasekhar S 1961 *Hydrodynamic and Hydromagnetic Stability* (Oxford: Clarendon)
[40] Landau L D and Lifshitz E V 1959 *Fluid Mechanics* (Oxford: Pergamon)